AIAA JOURNAL
Vol. 44, No. 2, February 2006

Summary of the 2004 Computational Fluid Dynamics Validation Workshop on Synthetic Jets

C. L. Rumsey,* T. B. Gatski,† W. L. Sellers III,‡ V. N. Vatsa,§ and S. A. Viken¶
NASA Langley Research Center, Hampton, Virginia 23681-2199

A computational-fluid-dynamics (CFD) validation workshop for synthetic jets and turbulent separation control (CFDVAL2004) was held in Williamsburg, Virginia, in March 2004. Three cases were investigated: a synthetic jet into quiescent air, a synthetic jet into a turbulent boundary-layer crossflow, and the flow over a hump model with no-flow-control, steady suction, and oscillatory control. This is a summary of the CFD results from the workshop. Although some detailed results are shown, the CFD state of the art for predicting these types of flows is mostly evaluated from a general point of view. Overall, for synthetic jets, CFD can only qualitatively predict the flow physics, but there is some uncertainty regarding how to best model the unsteady boundary conditions from the experiment consistently. As a result, there is wide variation among CFD results. For the hump flow, CFD is capable of predicting many of the particulars of this flow, provided that it accounts for tunnel blockage, but it consistently overpredicts the length of the separated region compared to the experimental results.

I. Introduction

THE study of separation control through the use of blowing, suction, and synthetic jets has been an active field of research for some time now.[1] Many experimental and theoretical papers (only a few of which this paper references) have been published on the subject.[2–6] The review paper by Greenblatt and Wygnanski[7] lists many additional references. There has also been a recent increase of attention paid to the field by AIAA, which held its first Flow Control Conference in June 2002 in St. Louis, Missouri, and now sponsors it as a continuing biennial series.

Computational methods have also been used extensively for computing synthetic jet flows. Only a few examples are referenced here.[8–13] However, it seems most computational-fluid-dynamics (CFD) efforts have been somewhat isolated, and so it has been difficult to make an assessment of the state of the art as a whole. To more broadly assess the current capabilities of different classes of computational methodologies, the time appeared to be ripe to hold a workshop for which many participants would compute the same flow control test cases. To this end, NASA Langley Research Center (LaRC) held the CFD Validation of Synthetic Jets and Turbulent Separation Control (CFDVAL2004) workshop in Williamsburg, Virginia, in March 2004.** Three different test cases, all of which were carried out experimentally at NASA LaRC, exercised various aspects related to the flow physics of separation control.

This paper is a summary report of the overall CFD results from the CFDVAL2004 workshop. It does not directly address technical issues associated with the experiments themselves, except as they relate to the CFD modeling of the flows. Measurement errors are not reported here for the unsteady cases, but estimates are given for uncertainty levels for the simpler (steady) hump case. Technical papers describing the experiments are also available[14–17] and provide additional details. This paper is organized as follows: first, a brief description of the workshop, including an overall description of the three test cases; then, a summary of results from each of the three test cases; finally, a summary and conclusions.

II. CFDVAL2004 Workshop

The CFDVAL2004 workshop was structured similarly to the series of refined turbulence modeling workshops sponsored by the European Research Community on Flow, Turbulence, and Combustion. Although not formally a part of the European series, CFDVAL2004 was held in association with ERCOFTAC, and representative members from that organization contributed to the workshop. CFDVAL2004 was also associated with the Air Force Office of Scientific Research, the International Association of Hydraulic Engineering and Research, QNET-CFD (a now-defunct European Union thematic network on quality and trust for industrial applications of CFD), and the National Institute of Aerospace.

There were 75 attendees at the workshop. Seven countries were represented, including the United States, France, Italy, Germany, Japan, the United Kingdom, and Switzerland. Most of the workshop participants came from universities, but some represented companies and public sector research laboratories as well.

The purpose of CFDVAL2004 was to bring together an international group of computational-fluid-dynamics practitioners to assess the current capabilities of different classes of turbulent flow solution methodologies to predict flowfields induced by synthetic jets and separation control geometries. The experimental data for the workshop were taken specifically with CFD validation in mind. Therefore, a great deal of effort was expended to attempt to document most of the relevant boundary conditions.

To encourage broad participation and to determine the general state of the art, the decision was made early not to dictate particular boundary conditions, grids, or method of solution. For example, although the experimental velocity was given as a function of time near the centers of the jet exits for cases 1 and 2, the participants had a choice as to the precise boundary condition used to try to match it. Although this strategy to broaden workshop participation was successful—solution methods ranged from reduced-order models through Reynolds-averaged Navier–Stokes (RANS) to large-eddy simulation (LES) and direct numerical simulation (DNS)—it also had an unavoidable downside. Differences in grids and boundary

Presented as Paper 2004-2217 at the 2nd Flow Control Conference, Portland, OR, 28 June–1 July 2004; received 20 August 2004; revision received 31 May 2005; accepted for publication 14 June 2005.

*Senior Research Scientist, Mail Stop 128, Computational Aerosciences Branch; c.l.rumsey@larc.nasa.gov. Associate Fellow AIAA.

†Senior Research Scientist, Mail Stop 128, Computational Aerosciences Branch; t.b.gatski@larc.nasa.gov. Member AIAA.

‡Branch Head, Mail Stop 170, Flow Physics and Control Branch; w.l.sellers@larc.nasa.gov. Associate Fellow AIAA.

§Senior Research Scientist, Mail Stop 128, Computational Aerosciences Branch; v.n.vatsa@larc.nasa.gov. Senior Member AIAA.

¶Technical Assistant of Systems Technology Development, Mail Stop 916, ASPO–Small Aircraft Transportation Systems; s.a.viken@larc.nasa.gov.

**Data available online at http://cfdval2004.larc.nasa.gov [cited 20 August 2004].

conditions represented an additional source of uncertainty when attempting to compare CFD results with each other.

The three test cases were chosen to represent different aspects of flow control physics. In test case 1 (synthetic jet into quiescent air), flow passed in and out of a slot (1.27 mm wide × 35.56 mm long) located on the floor of an enclosed box 0.61 m per side. A side-mounted circular piezoelectric diaphragm inside the cavity chamber beneath the floor drove the jet. The frequency was approximately 445 Hz, and the maximum velocity out of the slot was approximately 25–30 m/s. This case was considered to be nominally two dimensional at the center plane of the slot.

In test case 2 (synthetic jet in a crossflow), flow passed in and out of a circular orifice 6.35 mm in diameter. The orifice was located on the floor of a wind-tunnel splitter plate with a turbulent boundary layer at $M = 0.1$ and approximate boundary-layer thickness of 21 mm. The jet was driven electromechanically by a bottom-mounted, square-shaped, rigid piston mounted on an elastic membrane inside the cavity chamber beneath the splitter plate. The cavity was approximately 1.7 mm deep, and the piston moved approximately ±0.77 mm. The frequency was 150 Hz, and the maximum velocity out of the orifice was approximately $1.3U_\infty$.

In test case 3 (flow over a hump model), turbulent flow at $M = 0.1$ passed over a hump of chord 420 mm mounted on the floor of a wind-tunnel splitter plate. The hump used end plates at both sides (the model had a span of 584.2 mm between the plates), and the flow was nominally two dimensional in a wide region surrounding its center plane. The hump had a slot near 65% chord, near where separation naturally occurred. This case had two mandatory conditions: no flow control (no forced flow through the slot) and steady suction ($\dot{m} = 0.01518$ kg/s). There was also one optional condition (the experiment was not completed in time for the workshop) of oscillatory (synthetic) jet control. In this case, the jet was driven electromechanically by a bottom-mounted, rectangular-shaped, rigid piston mounted on an elastic membrane deep inside the cavity chamber. The frequency was 138.5 Hz, and the peak velocity out of the slot was approximately 27 m/s.

There was a great deal of CFD data submitted to this workshop. It is clearly not possible to show most of the results here. This report shows summary plots, as well as several specific detailed plots, that are representative of the solutions as a whole, or which serve to illustrate specific points or differences. Workshop participants were allowed to correct, resubmit, or withdraw their submissions during the month following the workshop; this paper summary contains the updated workshop information.

III. Case 1: Synthetic Jet into Quiescent Air

Table 1 gives a general tabulation of the submissions for case 1 (see Rumsey et al.[18] for additional details concerning each of the submissions). Eight contributors ran 25 separate cases. There was one LES submission, one reduced-order model submission, one two-dimensional blended RANS-LES submission, and several laminar Navier–Stokes submissions (the three-dimensional laminar runs perhaps can also be characterized as underresolved DNS); the others were unsteady RANS (URANS). Most of the runs were computed in two dimensions, but there were also a few three-dimensional computations. Note that none of the three-dimensional computations modeled the actual shape of the the cavity, including the circular diaphragm; instead, they were all computed using periodicity in the direction aligned with the slot's long axis. Six of the contributors modeled the cavity (or some approximation of the cavity), and two did not model any cavity. Of those who modeled the cavity, ONERA-flu3m and UKY-ghost applied a time-varying velocity on the side of the cavity where the diaphragm was located, derived from diaphragm-center displacement data. WASHU-wind and NASA-tlns3d also applied a similar boundary condition there but based it on the best matching of the data at the slot exit. GWU-vicar3d used a different cavity shape with time-varying velocity boundary condition applied at the bottom wall. NCAT-quas1d modeled the motion of the actuator with a quasi-one-dimensional model.

All of the results were calculated with structured grids. Only two contributors (UKY-ghost and NASA-tlns3d) ran with the same grid, two dimensions with approximately 64,000 points. This grid, along with other structured and unstructured grids, was made available to participants several months before the workshop.

This section shows the comparison of the results for case 1 with particle image velocimetry (PIV) and hot-wire data. Other experimental data were later taken using a different piezoelectric diaphragm. (These devices are prone to occasional failure.) These later data also include laser-Doppler-velocimetry (LDV) measurements in addition to PIV and hot wire, but they were also at slightly different conditions (higher maximum outflow velocity) than the data used for the workshop. This report shows only the original data used by the participants in the workshop. The later data are given in Yao et al.[14] Figure 1 gives a sketch showing the locations of most of the submitted results from the computations, and Fig. 2 gives the definition of the jet width used for this case.

Time histories of v velocities near the center of the slot exit are shown in Fig. 3. Recall that the different contributors used different

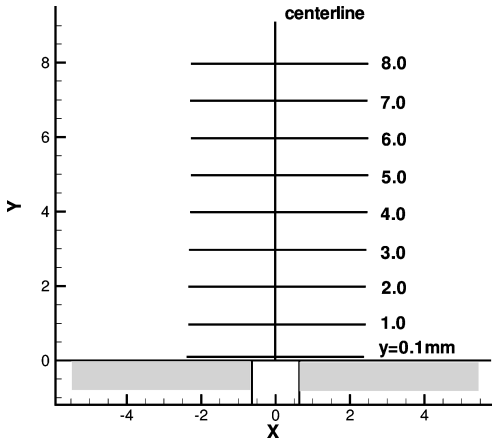

Fig. 1 Sketch of the case 1 comparison locations.

Table 1 Case 1 summary of submissions

Label	Organization/ lead author	Method	Grid sizes
ONERA-flu3m	ONERA/Mary	LES, Lam. N-S, URANS (SA)[a]	52 K(2-D), 930 K(3-D)[b]
UKY-ghost	U. Kentucky/Huang[c]	URANS (SST)	64 K, 199 K(2-D)
GWU-vicar3d	GWU/Rupesh	Lam. N-S	465 K, 697 K(3-D)
NCAT-quas1d	NC A&T State U. and NASA LaRC/Yamaleev	Reduced-order mod. in slot+4th ord. Lam. N-S	98 K(2-D)
POIT-saturne	U. Poitiers/Carpy	URANS (k-e, RSM)	16 K, 63 K(2-D)
WARWICK-neat	U. Warwick and U. Wales/Preece	URANS (k-e, nonlin. k-e, EASM)[d]	5 K(2-D)
WASHU-wind	Washington U./Cui	URANS (SA, SST, SST-LES)	36 K(2-D)
NASA-tlns3d	NASA LaRC/Vatsa	URANS (SA, SST)	16 K, 64 K, 88 K(2-D)

[a]N-S = Navier–Stokes. [b]2-D, 3-D, = two- and three-dimensional. [c]U. = University. [d]EASM = explicit algebraic stress model.

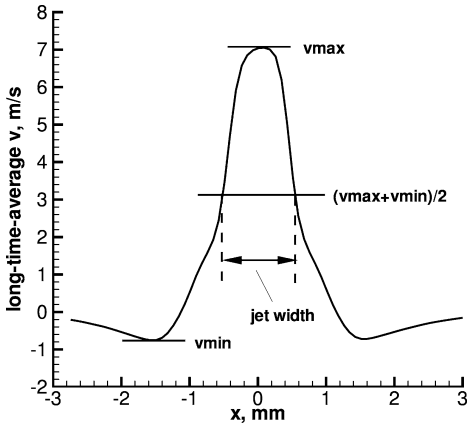

Fig. 2 Sketch showing definition of jet width for case 1.

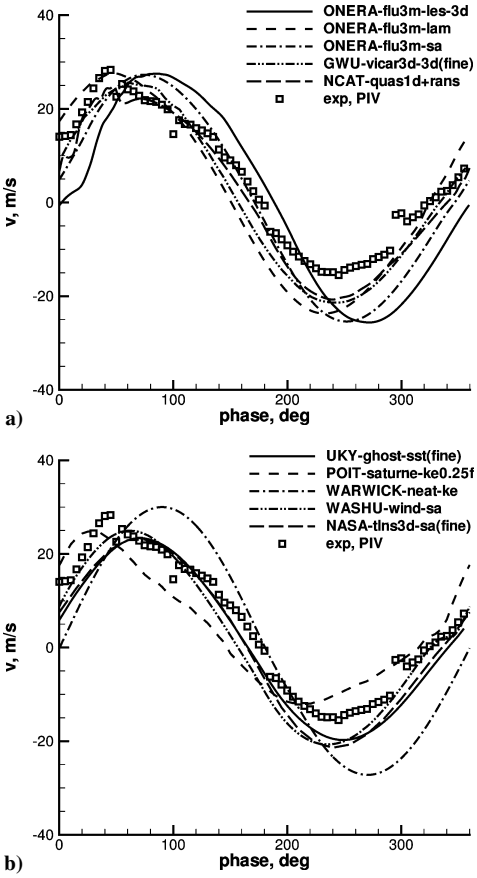

Fig. 3 Case 1 time histories of v velocity at $x = 0$, $y = 0.1$ mm; for ease of readability, results are divided into two figures.

unsteady boundary conditions; this is likely a contributing cause of the large variation in the CFD results. Although both PIV and hot-wire measurements were available at this location, only PIV data are shown here because the hot-wire data at this near-slot location exhibited unphysical behavior. Note that the experimental measurements indicated approximately a 200-deg phase difference between peak and trough, whereas most of the CFD methods yielded 180 deg. Some of the differences in particular phase-averaged results between CFD and the experiment could be a result of not matching the same phase.

Figure 4 shows long time-average v-velocity profiles along the centerline, $x = 0$. One can see a significant difference between the two measurement techniques very near the slot for y less than approximately 2 mm. The reason for this difference is not known. Individual uncertainty errors for each of the two measurement

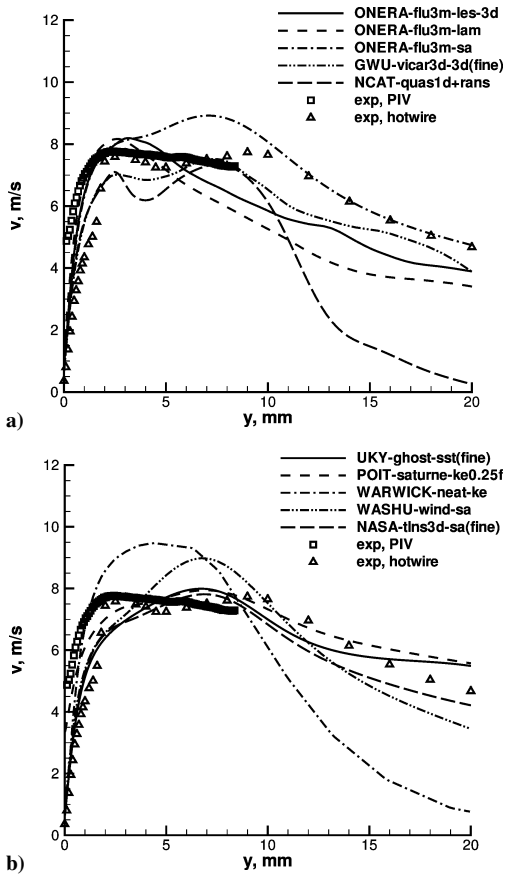

Fig. 4 Case 1 average v-velocity profiles at $x = 0$; for ease of readability, results are divided into two figures.

techniques (approximately 1–2% for PIV and 6% for hot wire near the slot) were less than the difference seen in the wall region. This type of measurement discrepancy is an active area of experimental research for synthetic jet flows (see Yao et al.[14] for additional discussion). Significant variations also existed between the CFD results over the entire y range. Most of them showed similar trends to the experiment, although NCAT-quas1d and WARWICK-neat indicated a more rapid drop in velocity for $y > 10$ mm compared to the other results.

Long time-average results along two $y =$ constant lines ($y = 0.1$ and 4 mm, respectively) are shown in Figs. 5 and 6. Just above the slot exit, at $y = 0.1$ mm, all results except POIT-saturne greatly underpredicted the average jet magnitude. However, beginning near 1–2 mm and above, all of the CFD results agreed very well with the PIV experiment. Figure 6 shows an example of this better agreement at $y = 4$ mm. There was relatively little spread among the CFD results at this location. Although not shown, the variation between the CFD results increased at higher y stations, which was probably primarily a result of differences in numerical dissipation caused by the use of different grid sizes and turbulence models.

Figure 7 shows the long time-average jet width. Most CFD results tended to somewhat overpredict the width. The ONERA-flu3m laminar result was similar to the other methods near to the wall but then predicted too much spreading of the jet past $y = 4$ mm. It was more than twice as wide as the experimental results near $y = 8$ mm. Although not shown, the CFD results had significantly greater variation for $y > 8$ mm.

For the sake of brevity, only one representative phase-averaged result is shown here. Figure 8 shows v-velocity profiles at $y = 4$ mm, at phase $= 135$ deg. Compared with the long time-average results shown earlier, this typical phase-averaged result illustrates that there was a great deal more CFD variation at this level of detail. Also, the comparison was not as good with experimental data.

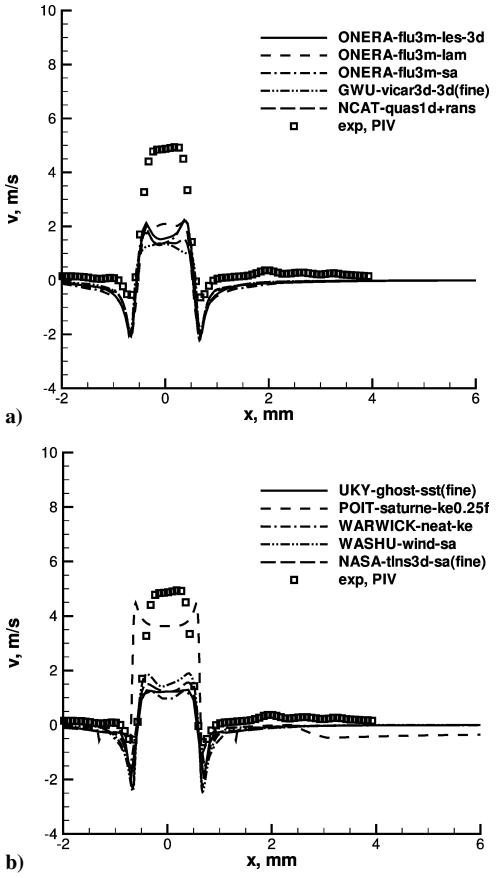

Fig. 5 Case 1 average v-velocity profiles at $y = 0.1$ mm; for ease of readability, results are divided into two figures.

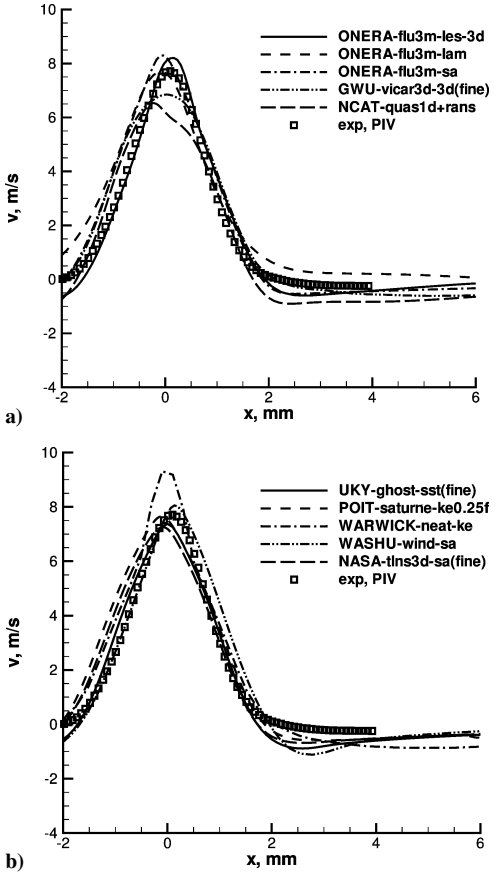

Fig. 6 Case 1 average v-velocity profiles at $y = 4$ mm; for ease of readability, results are divided into two figures.

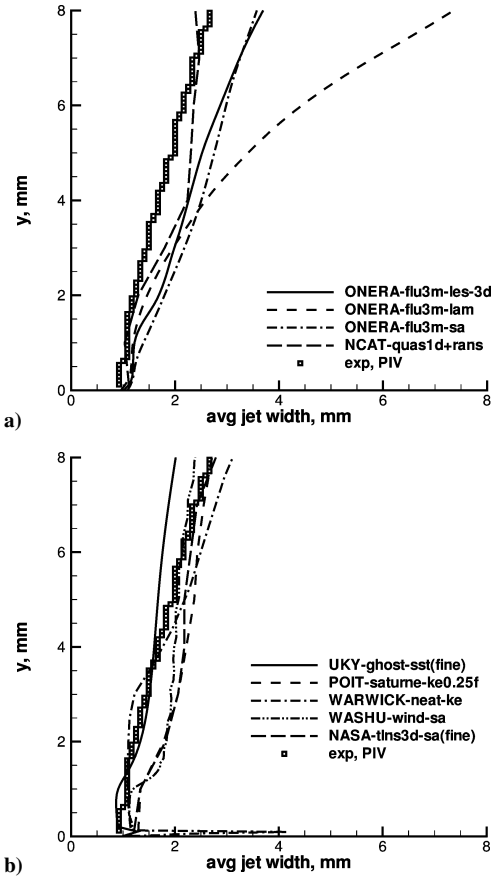

Fig. 7 Case 1 jet width based on average v velocity; for ease of readability, results are divided into two figures.

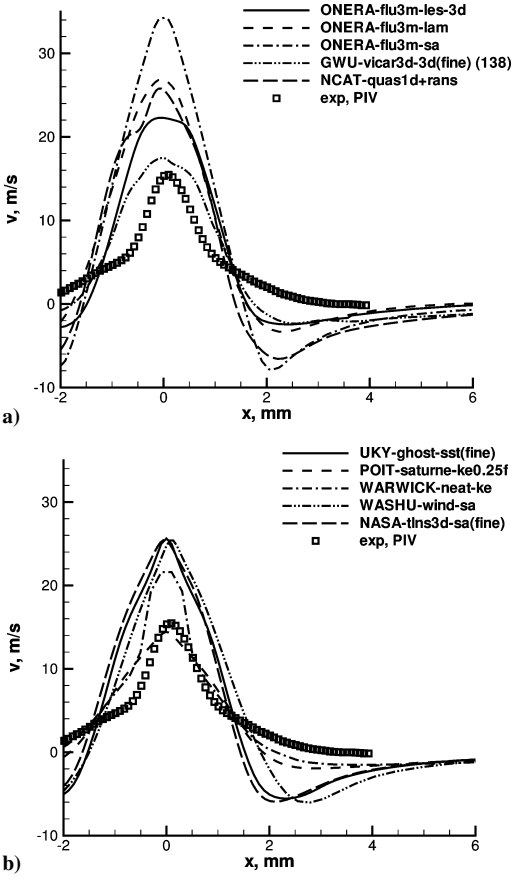

Fig. 8 Case 1 phase-averaged v-velocity profiles at $y = 4$ mm, phase = 135 deg; for ease of readability, results are divided into two figures.

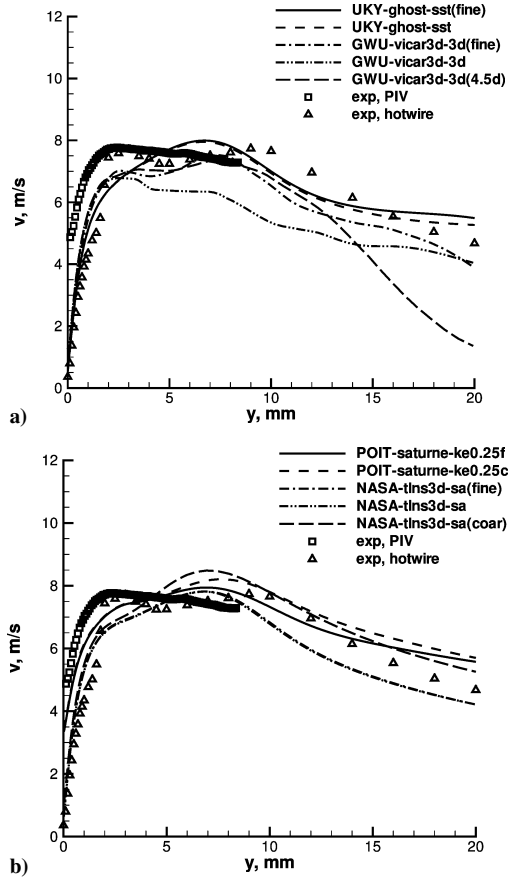

Fig. 9 Grid effect on case 1 average v-velocity profiles at $x = 0$; for ease of readability, results are divided into two figures.

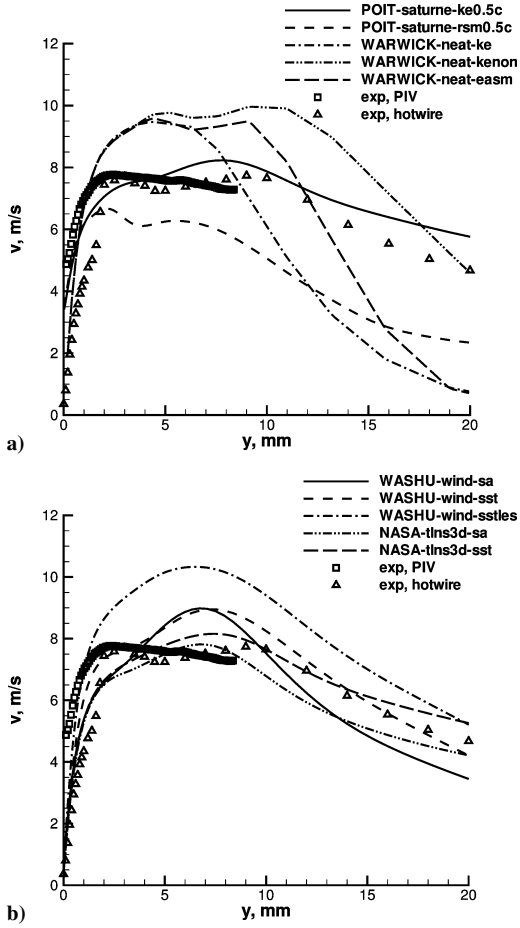

Fig. 10 Turbulence model effect on case 1 average v-velocity profiles at $x = 0$; for ease of readability, results are divided into two figures.

Several participants investigated the effect of time step and grid size on the solution. Although not shown, time step had very little effect for any of the solutions. The effect of the grid was relatively small near the wall, but it could be larger away from the wall. This is illustrated in Fig. 9, which shows long time-average v velocity along the centerline. UKY-ghost and POIT-saturne showed only minor variation, but grid size and its spanwise extent affected the 3-D GWU-vicar3d results. NASA-tlns3d fine and medium grids gave nearly identical results, but the coarse grid was different.

The turbulence model's effect on the CFD results was found to be fairly significant for this case. Figure 10 shows the results. For POIT-saturne, the $k-\varepsilon$ model compared better with experimental data than the Reynolds-stress model for this quantity. For WARWICK-neat, three different turbulence models were essentially the same for $y < 4$ mm, but then they behaved very differently beyond that. None of these agreed particularly well with experimental data, but WARWICK-neat used a very coarse grid with less than 5000 points. For WASHU-wind, Spalart–Allmaras (SA) and Menter's shear-stress transport (SST) were fairly similar, especially for $y < 7$ mm, but the two-dimensional blended SST–LES method generally overpredicted the average velocity everywhere. For NASA-tlns3d, SA and SST showed similar variation to that seen by WASHU-wind: the two models were close near the wall, then SST predicted somewhat larger velocities than SA farther from the wall.

Although not shown, the computed turbulence quantities (e.g., $u'v'$) did not compare well at all with experimental data, and there were very large variations exhibited among CFD results. Also, there is some question whether the measured data are entirely a result of turbulence or a result of unsteady "flapping" of the time-dependent jet. The participants of the workshop generally felt that this case 1 flow is probably laminar in the beginning, then transitional further into the flowfield. Therefore, the use of a standard RANS turbulence model might not be entirely warranted.

As mentioned earlier, many of the participants had difficulty matching the nonsinusoidal v-velocity phase variation at the slot outflow (see Fig. 3). As a result, at certain phases they found that the computed jet could be at a different position than in the experiment. This is illustrated by example flowfield contours at phase = 135 deg, shown in Fig. 11. Similar to most other results (not shown), the NASA-tlns3d result at this phase had the extent of its peak jet velocity lower (near 4 mm) than seen in the experimental data (near 7 mm). It is also possible that three-dimensional effects caused by ring vortices formed from the slot ends had an influence on the flowfield in the experiment, especially at distances far from the wall.

There did not appear to be a distinct advantage to modeling the cavity for this case, as opposed to specifying a jet boundary condition at the surface. Regarding grid effect, two-dimensional grid levels of about 60,000 points (including cavity) were found to be sufficient to resolve the computed flow physics, whereas 16,000 points yielded noticeable differences in the solution. Among three-dimensional results, changing from 460,000 to 700,000 points (or increasing the spanwise periodic extent) could significantly alter the solution far into the flowfield. Very little effect resulted from changing the time step, even with as few as 72 steps per period.

IV. Case 2: Synthetic Jet in a Crossflow

Table 2 gives a general tabulation of the submissions for case 2 (see Rumsey et al.[18] for additional details concerning each of the submissions). Five contributors ran 10 separate cases. There was one LES submission; the others used URANS. All runs were (necessarily) three-dimensional. All methods were second order in space and time. All submissions modeled the cavity, except for CIRA-zen, which specified a time-varying profile at the orifice exit. However, both USTO-rans and NASA-fun3d altered the cavity shape. In the latter case, the bottom wall was made flat while keeping

Table 2 Case 2 summary of submissions

Label	Organization/ lead author	Method	Grid sizes
NASA-cfl3d	NASA LaRC/ Rumsey	URANS (SA, SST, EASM)	490 K, 3.9 M (3-D)
USTO-rans	USTO and ETH/ Azzi	URANS (TLV, EASM)	210 K(3-D)
ONERA-flu3m	ONERA/ Dandois	LES	1.7 M(3-D)
CIRA-zen	CIRA/ Marongiu	URANS (k-e)	776 K(3-D)
NASA-fun3d	NASA LaRC/ Atkins	URANS (SA)	46 K, 260 K (3-D)

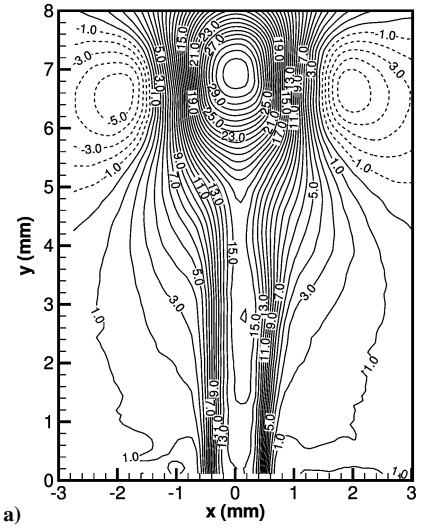

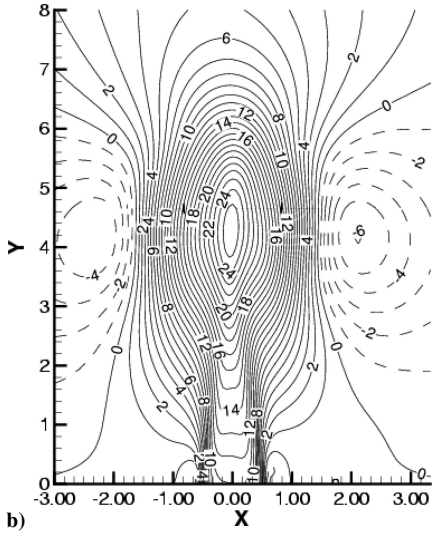

Fig. 11 Case 1 contours of v-velocity, phase = 135 deg; a) PIV experiment and b) NASA-tlns3d-sa(fine).

the volume the same as the original (stepped) geometry. Two of the contributors modeled the full plane, while the others modeled a half-plane with symmetry imposed at the center plane. Each contributor used a different grid: four used structured grids and one (NASA-fun3d) used unstructured. The four contributors who modeled the cavity applied a time-dependent velocity specification at the cavity bottom wall: $\tilde{V} = V\cos(2\pi f t)$. Each adjusted V to achieve what was considered to be a reasonable match of the experimental w-velocity variation at the orifice exit.

This report quantitatively compares case 2 results only to LDV data. A sketch showing some of the LDV data measurement locations is given in Fig. 12. PIV data were also acquired at several planes. The reader interested in quantitatively comparing experimental results using the two different techniques should refer to Schaeffler and Jenkins.[15] In that reference, it was shown that

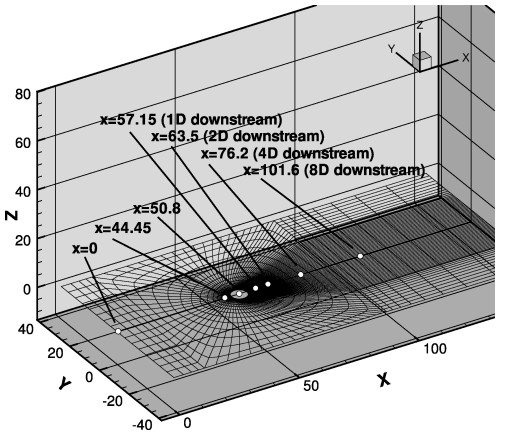

Fig. 12 Sketch of some of the case 2 comparison locations.

individual uncertainty errors for each of the two techniques could be smaller than the measured differences at certain locations and phases. (For example, the measured LDV and PIV u velocity differed by as much as 20% during the expulsion part of the cycle at a particular position over the orifice, but the combined uncertainty error in each measurement was less than this difference.) As mentioned in the last section, this type of measurement discrepancy is an active area of experimental research for synthetic jet flows.

Figure 13 shows the time histories of velocities near the center of the orifice exit. Recall that the different contributors used different unsteady boundary conditions; this is likely a contributing cause of the large variation in the CFD results. The u-velocity component was captured well by three of the codes. CIRA-zen showed a higher value, and NASA-fun3d showed a lower value than experimental results during the expulsion part of the cycle. (Although not shown here, the lower NASA-fun3d result was later determined to be caused by its particular boundary condition employed, which allowed tangential velocity to develop at the bottom cavity wall. Changing its boundary condition to be similar to other codes resulted in better agreement.)

All codes predicted a zero or near-zero cross-stream v component of velocity, whereas the experimental data indicated a very large v component during expulsion. The cause of this high experimental value is not known. Cavity resonances might have had an influence, and the measurements might have been taken slightly off center, but even these explanations are unlikely to account for such a large magnitude. It is possible that some aspect of the experimental setup was asymmetric enough to cause a significant sideways component of velocity at the exit plane. Finally, all codes captured the w velocity reasonably well (with some variation), although no one replicated the "dip" near phase = 160 deg. The cause for this dip in the experimental result is also not known. The cavity under the orifice was extremely shallow (nominally 1.7 mm deep neutral position with tunnel on), and the piston moved ± 0.77 mm up and down from this position. The volume in the cavity more than doubled from roughly 10,000 to 26,000 mm^3 during the cycle. It is questionable whether a simple nonmoving wall transpiration boundary condition, used by all of the CFD methods, is a very accurate model for this large of a range of piston motion.

Figure 14 shows long time-average u-velocity profiles on the center plane at three downstream stations. Overall, there was fair agreement between CFD and the experiment, but there was also a significant spread among the CFD results. In particular, each method qualitatively portrayed the relative magnitude and height of the velocity inflection at each x location. However, no one method yielded consistent agreement with the experiment throughout the boundary layer. Figure 15 shows w-velocity profiles along one spanwise line and two streamwise lines. Along the spanwise line (where no experimental LDV data were taken) there was a significant spread in the CFD results. Note that four of the CFD results were either symmetric about $y = 0$ or else assumed symmetry. However, the ONERA-flu3m (LES) result, averaged in time, showed a slight

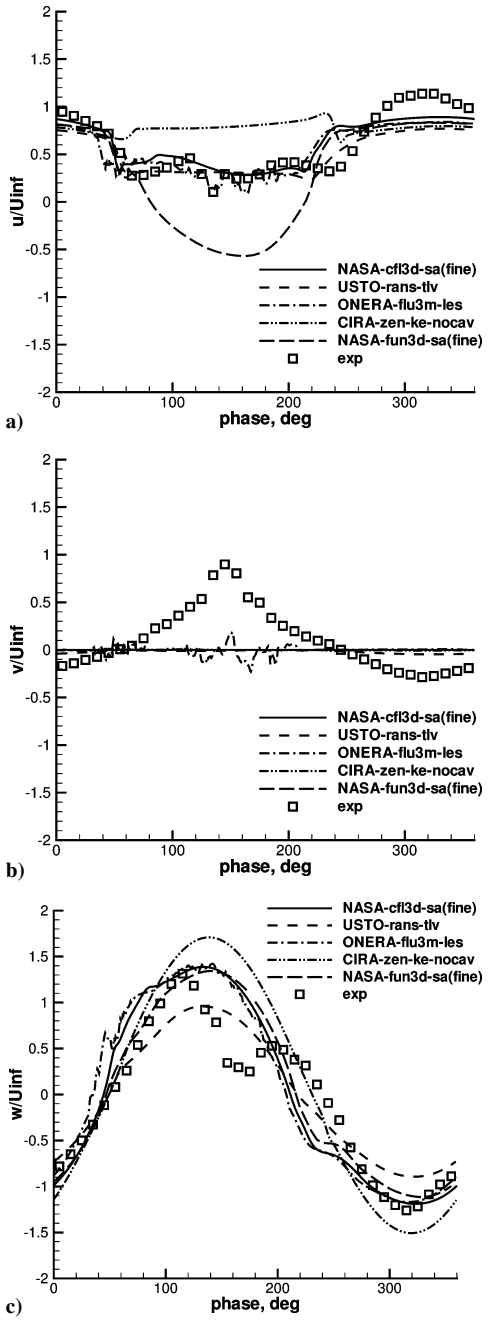

Fig. 13 Case 2 time histories at $x = 50.63$ mm, $y = 0$, $z = 0.4$ mm: a) u velocity, b) v velocity, and c) w velocity.

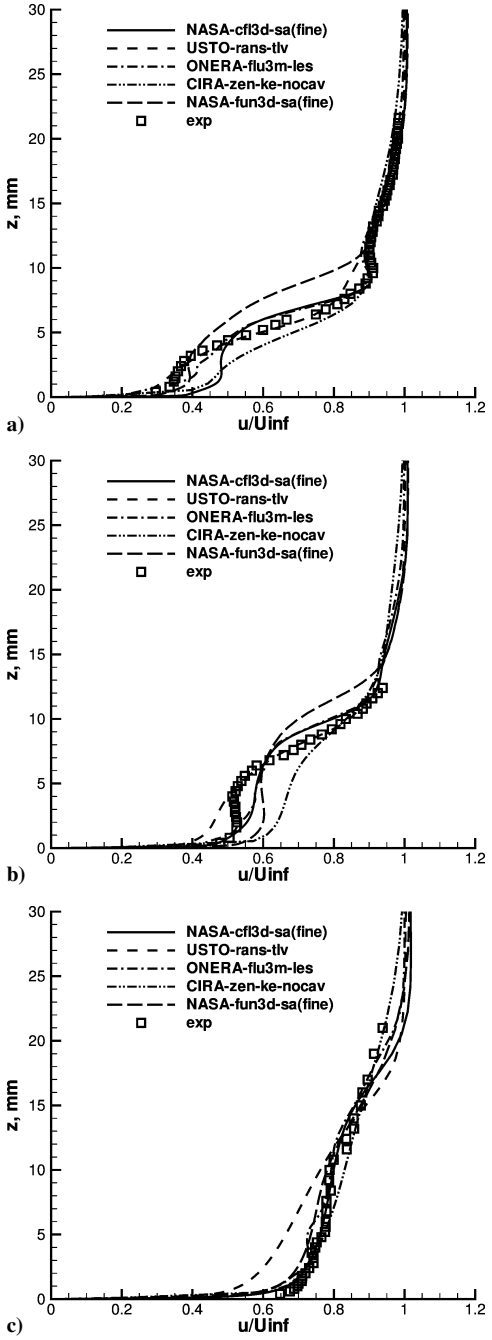

Fig. 14 Case 2 average u velocity at $y = 0$: a) one diameter downstream, b) two diameters downstream, and c) eight diameters downstream.

deviation from symmetry. Along the streamwise lines, the five CFD results again exhibited significant spread; two of the CFD methods exhibited reasonably good agreement with experimental results along the $z = 10$ mm, $y = 0$ line (Fig. 15c).

Two of the participants examined the effect of grid size on the solution. The results can be briefly summarized in a representative figure, Fig. 16. In general, the fine (3.9 million cells) and coarser (490,000 cells) grids used in NASA-cfl3d did not exhibit a dramatic influence on the solution. However, for NASA-fun3d the fine (260,000 nodes) and coarser (46,000 nodes) grids did show a significant difference.

Two of the participants investigated the effects of different turbulence models on the solution. Again, only one representative figure is shown here for the sake of brevity, Fig. 17. In NASA-cfl3d, three different models resulted in minor differences from each other, but none was clearly better in comparison with the experimental data. The two models used by USTO-rans also showed only minor differences from each other, and they were clearly different in character from both the NASA-cfl3d results and the experimental data. In other words, the turbulence models themselves did not have as much of an impact as the combined effect of different codes, grids, and other solution variations.

This report only shows a few phase-averaged results. Figure 18 shows u velocity along a line one diameter downstream at three different phases. All CFD results were in good agreement with each other and with experimental results at phase = 0 deg. (At this time the orifice is still in its suction phase, and so there is little to no dynamic flow occurring one diameter downstream.) However, at the two later phases the influence of the expulsion part of the cycle is felt at this location. The CFD results captured the influence, generally following the trends seen in the experiment but with a significant spread in the solutions.

Phase-averaged turbulence quantities from the CFD solutions generally exhibited similar trends to each other, but again with a significant spread. There were usually larger discrepancies between

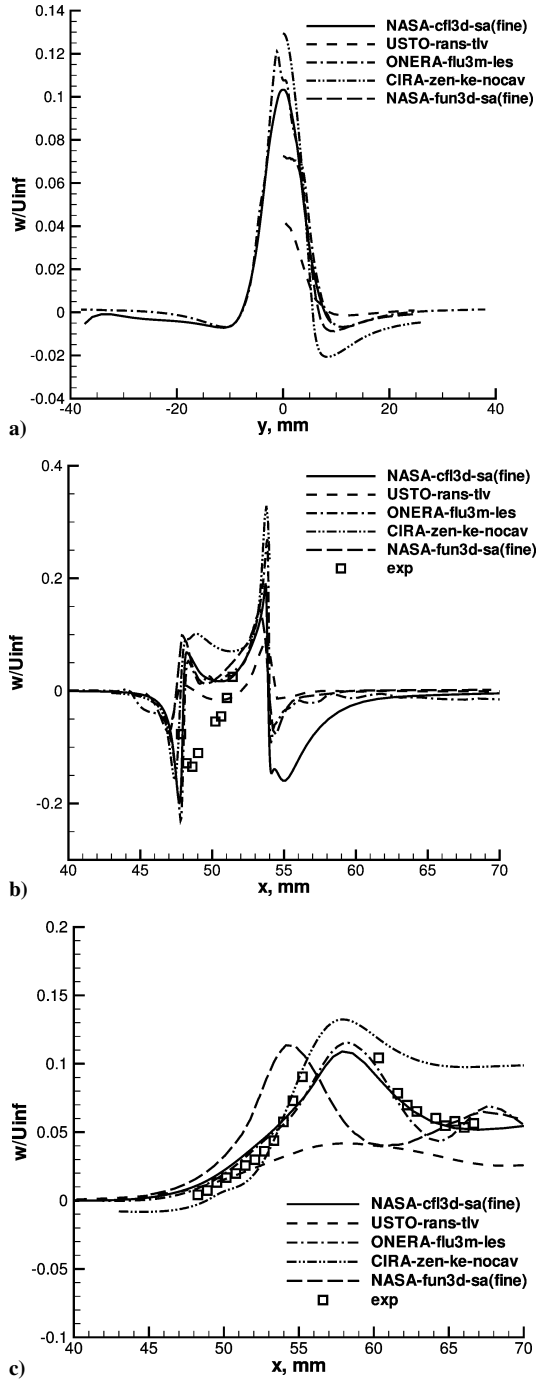

Fig. 15 Case 2 average w velocity: a) $z = 10$ mm one diameter downstream, b) $z = 0.4$ mm and $y = 0$, and c) $z = 10$ mm and $y = 0$.

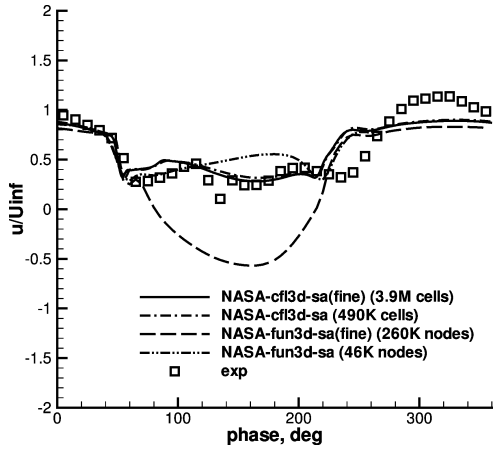

Fig. 16 Grid effect on case 2 u-velocity time histories at $x = 50.63$ mm, $y = 0$, $z = 0.4$ mm.

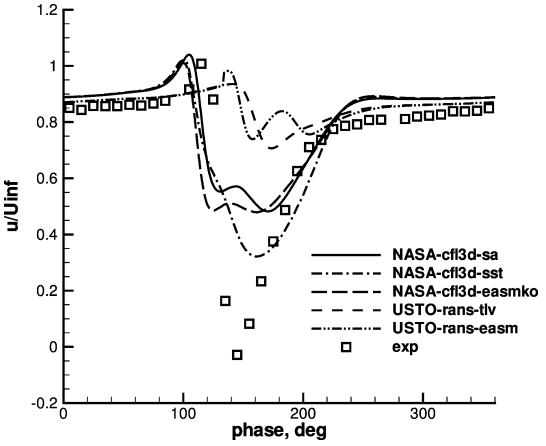

Fig. 17 Turbulence model effect on case 2 u-velocity time histories at $x = 63.5$ mm, $y = 0$, $z = 10$ mm.

CFD and the experiment than the discrepancies seen between the turbulence models. Figure 19 shows an example.

Finally, Fig. 20 shows a sample comparison between experiment and CFD over the entire plane one diameter downstream. This figure shows u-velocity contours at phase = 120 deg. It is intended as a qualitative comparison only. Also, only one CFD result is shown for brevity; other CFD results were qualitatively similar. Although details were different, this figure indicates that CFD predicted the overall structure of the dynamic flow resulting from the expulsion part of the cycle as it passes downstream.

For this case study, LES vs URANS did not appear to be a significant factor. In fact, overall (in a subjective sense) the two methods that tended to yield the most similar long time-average and phase-averaged mean-flow solutions were ONERA-flu3m (LES) and NASA-cfl3d (URANS). In general, no one method, algorithm, or turbulence model stood out as being the best methodology for capturing the physics of this flow. Grid levels of about a half a million points or more appeared to be sufficient to capture the general character of the unsteady flow sufficiently well, whereas grids coarser than this could change the solution significantly. None of the participants submitted results examining the effect of time step; however, NASA-cfl3d performed computations varying between 720 and 1440 steps per cycle that were not submitted, and found very little effect.

V. Case 3: Flow over a Hump Model (Separation Control)

A general tabulation of the submissions for case 3 is given in Table 3 (see Rumsey et al.[18] for additional details concerning each of the submissions). There were 13 contributors who ran 56 separate cases. Methods were mostly RANS and URANS, but one was a DNS result (underresolved very near the wall), and several were blended RANS–LES results. Most of the runs were computed in two dimensions, but several were three-dimensional computations. Various spatial orders of accuracy were employed, with the majority second order. Some of the three-dimensional computations were periodic in the spanwise direction, and some were half-plane (either flat inviscid side-wall or actual side-plate geometry modeled viscously). Most of the contributors modeled the cavity, but several applied boundary conditions directly on the hump surface. Contributors computed results on both structured and unstructured grids. Many used the two-dimensional grids supplied by the workshop organizers. The supplied structured grid had approximately 208,000 cells (fine) and 52,000 cells (coarse). The supplied unstructured

Table 3 Case 3 summary of submissions

Label	Organization/ lead authors	Method	Grid sizes
AFRL-fdl3di	OAI and AFRL/Morgan[a]	RANS (k-e)	50 K, 200 K(2-D), 2.6 M(3-D)
AZ-cobalt	Arizona State and Cobalt Solutions/Krishnan	DES, RANS (SA, SST)[b]	Various 52 K–254 K(2-D), 2.6 M–10.7 M(3-D)
BOEING-overflow	Boeing/Shmilovich	RANS (SA, SST)	48 K(2-D)
META-cfd++	Metacomp Tech/Shariff	RANS (cubic k-e), LNS[c]	1.8 M, 2.5 M(3-D)
CIRA-zen	CIRA and CTR/Marongiu[d]	RANS (SST, k-e)	144 K, 171 K(2-D)
CTR-fluent	CIRA and CTR/Marongiu	RANS (SA)	49 K, 198 K(2-D)
NASA-cfl3d	NASA LaRC/Rumsey	RANS (SA, SST, EASM)	52 K, 208 K(2-D)
NASA-rans	NASA LaRC/Balakumar	RANS (SST)	103 K(2-D)
NASA-fun2d	NASA LaRC/Viken	RANS (SA)	57 K, 124 K(2-D)
UAZ-cfl3d	U. Arizona/Israel	FSM w/lin. EASM[e]	2.8 M(3-D)
UAZ-DNS	U. Arizona/Postl	DNS	105 M(3-D)
UK-ghost	U. Kentucky/Katam	RANS (SST)	49 K, 198 K(2-D)
UMD-rans	U. Maryland/Duraisamy	RANS (SA, SST)	52 K, 208 K(2-D), 2.1 M(3-D)
US-fluent	Utah State/Spall	RANS (k-o, k-e, SA, SST, v2f)	86 K(2-D)

[a]OAI = Ohio Aerospace Institute, AFRL = Air Force Research Lab. [b]DES = detached eddy simulation. [c]LNS = limited numerical scales. [d]CIRA = Centro Italiano Ricerche Aerospaziali, CTR = Center for Turbulence Research. [e]FSM = flow simulation methodology.

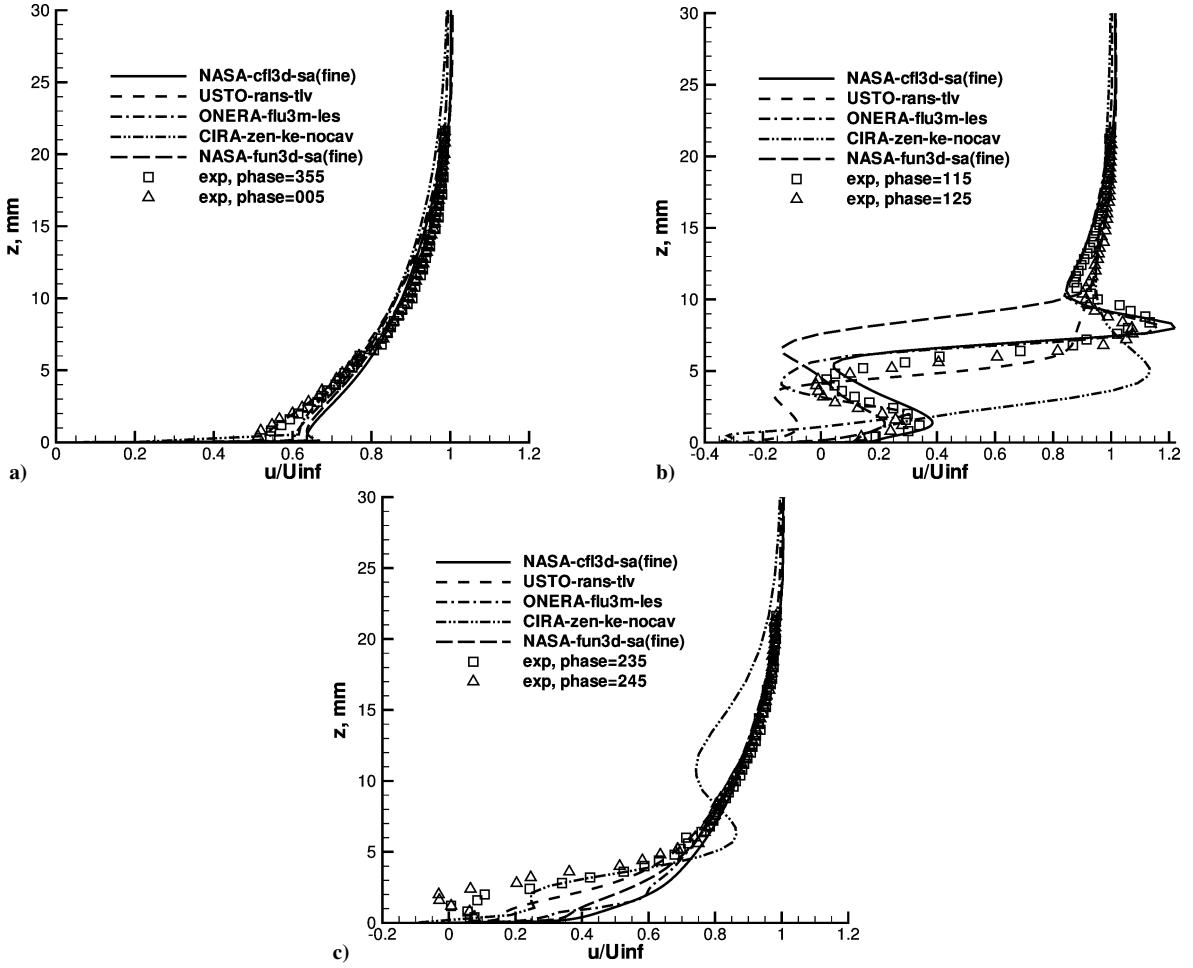

Fig. 18 Case 2 phase-averaged u velocity at $y = 0$ and one diameter downstream: a) phase = 0 deg, b) phase = 120 deg, and c) phase = 240 deg.

grid had approximately 124,000 nodes and 247,000 cells (fine) and 57,000 nodes and 114,000 cells (coarse).

Case 3 is different from cases 1 and 2 in that most of the results were not time dependent. Only the optional oscillatory-control case was unsteady, and, for that case only long time-average Cp were requested from the participants. (Eight of the contributors computed this, running 12 separate cases.) However, more extensive time-dependent data became available after the workshop; thus, the oscillatory-control experiment can serve as a good test case for future time-accurate validation exercises. Figure 21 gives a sketch showing the locations of most of the submitted computational results. Computed pressure coefficients are compared with experimental data from surface-mounted pressure taps, and velocity and turbulence profiles are compared with PIV experimental data. The measured pressure coefficients were accurate to ± 0.001, the measured velocity uncertainty was less than 3%, and the worst-case uncertainty error in turbulence quantities was approximately $\pm 10\%$. Greenblatt et al.[16,17] report the experimental details.

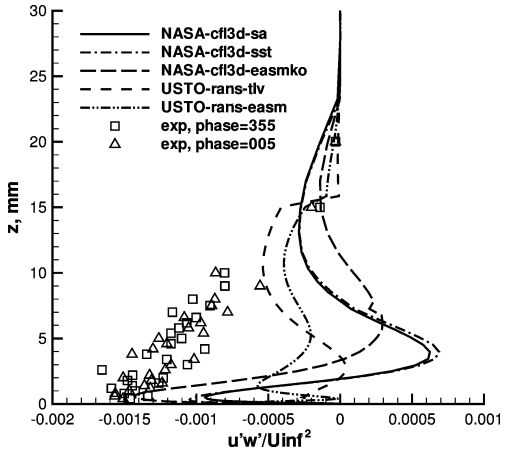

Fig. 19 Turbulence model effect on case 2 phase-averaged $u'w'$ turbulent stress at $x = 44.45$ mm, $y = 0$, phase = 0 deg.

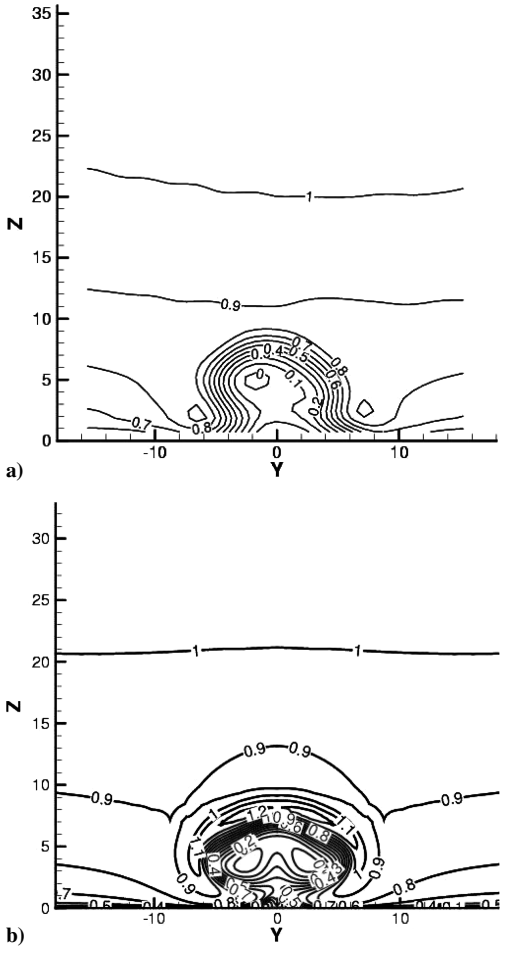

Fig. 20 Example contours of phase-averaged u velocity, one diameter downstream, phase = 120 deg: a) PIV experiment and b) NASA-cfl3d-sa(fine).

A summary of all of the CFD results for the no-flow-control condition is shown in Fig. 22. (Note that the figure does not display the separation and reattachment locations for those methods that did not report skin friction.) As a whole, most CFD results missed the pressure levels over the hump between $0.2 < x/c < 0.6$ and also predicted higher pressures than experimental results in the separated region upstream of $x/c = 1$. As will be shown next, the missed pressures were likely caused by blockage effects caused by the side plates in the experiment. The separation location (not known precisely for the experiment) was predicted reasonably well by most

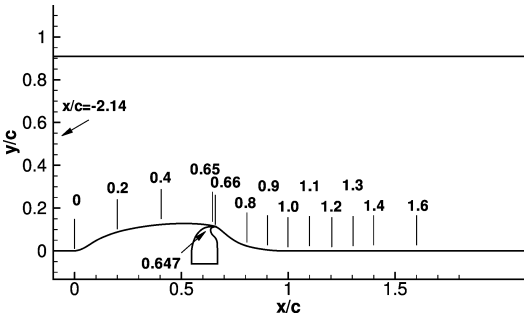

Fig. 21 Sketch of the case 3 comparison locations.

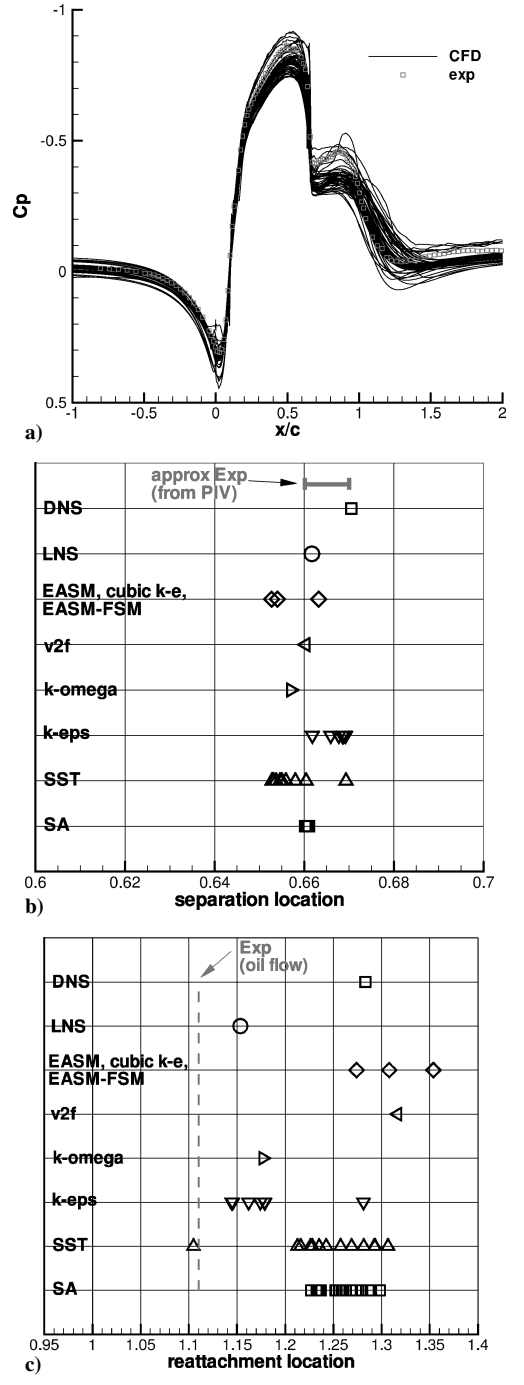

Fig. 22 Summary of case 3 results compared to experimental data for no-flow-control condition: a) *Cp*, b) separation location, and c) reattachment location.

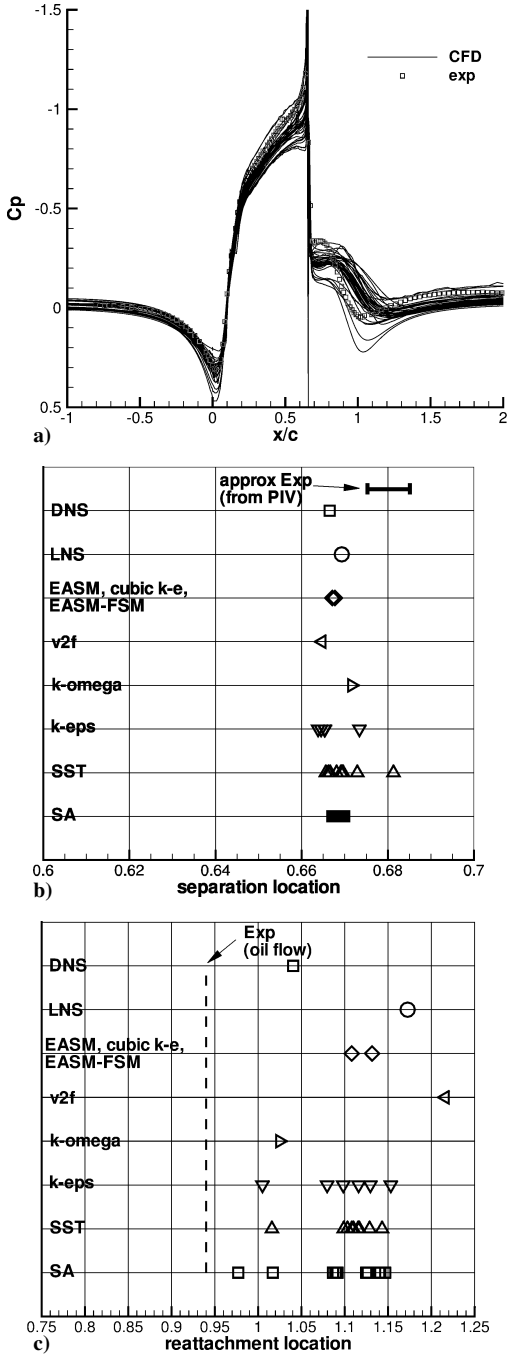

Fig. 23 Summary of case 3 results compared to experimental data for suction condition: a) *Cp*, b) separation location, and c) reattachment location.

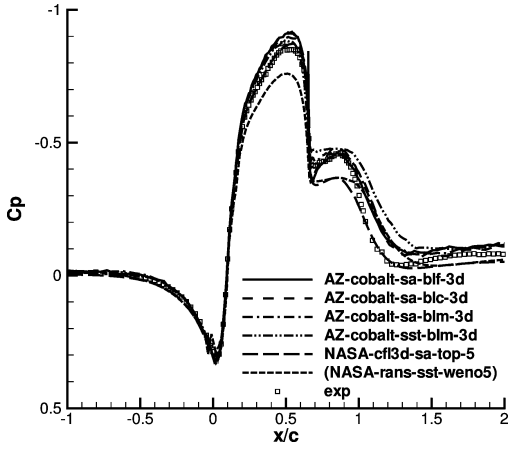

Fig. 24 Surface-pressure coefficients for case 3 results that accounted for tunnel blockage. (For comparison, one result, NASA-rans-sst-weno5, is shown that did not account for blockage.)

CFD methods, and the reattachment location was predicted (for the most part) significantly downstream of the experimental location of $x/c = 1.11$. Most models of similar type generally behaved similarly. Two exceptions were CIRA-zen-sst-kprof-3, which predicted separation later and reattachment earlier than other results with the SST model, and CIRA-zen-ke, which predicted reattachment farther downstream than other results using a $k-\varepsilon$ model. CIRA-zen also reported unusually low skin-friction levels for all of its results.

Figure 23 shows a summary of all of the CFD results for the steady suction condition. Again, most CFD results overpredicted the pressure levels over the hump between $0.2 < x/c < 0.6$. Also, the pressures in the separated region did not exhibit the same levels or shape as experimental results. The separation location (again not known precisely for the experiment) was predicted to be slightly upstream of the experimental location, and the reattachment location was predicted to be significantly downstream of the experimental location of $x/c = 0.94$ by all CFD methods. For the suction condition, the results generally exhibited a broader range for a given turbulence model than for the no-flow-control condition. Notable results that showed the largest differences from other turbulence models of the same type were CTR-fluent-sa-2, CTR-fluent-sa-1, NASA-rans-sst-weno5, and US-fluent-ke.

Figures 22 and 23 are also instructive from the point of view of CFD uncertainty. The surface-pressure coefficient plots illustrate the range of variation of CFD for these cases. This variation is caused by use of different grids, codes, turbulence models, and boundary conditions (including two- vs three-dimensional modeling).

The tendency for most of the CFD results to miss the pressure levels over the front half of the hump was believed to be caused by blockage effects in the experiment. Two pieces of evidence support this conjecture. First, the three-dimensional AZ-cobalt runs that accounted for the side-plate physical shape (modeled as a viscous wall) resulted in improved levels there. Second, the two-dimensional NASA-cfl3d run that used an altered top wall shape to approximately account for the side-plate blockage (using area ratio of plate cross section to tunnel cross section) resulted in excellent agreement of pressures over the front part of the hump compared with experimental data. Figure 24 shows these results (one of the standard "uncorrected" results is also included for comparison). From this figure the three-dimensional AZ-cobalt runs also yielded good results in the separated region, whereas the two-dimensional NASA-cfl3d runs did not. This suggests that there might be small three-dimensional separated wall-juncture structures along the back end of the side plates that further constrict the flow (additional blockage) in the separated region.

Although not shown, most of the contributed results were in fairly good agreement with experimental data (for both velocity profiles and turbulent shear-stress profiles) just upstream of the slot (especially for the no-flow-control condition). The velocity profiles inside the separated region were also predicted reasonably well, on the whole, for both no-flow-control and suction conditions. However, because the CFD results reattached too late, most velocity profiles compared poorly with experimental data at stations downstream of reattachment. The two exceptions to this were AZ-cobalt-des-1-3d and META-cfd++lns-3d, which agreed well with experiment for the no-flow-control condition. Profiles using these methods (along with five other typical representative solutions) at $x/c = 1.2$ are shown in Fig. 25. However, all results were poor downstream of reattachment for the suction condition. Figure 26 shows 14 representative results at $x/c = 1.0$. Note that the experimental uncertainty in the measured velocity in these case 3 profile plots is generally on the order of the symbol size used.

A possible reason for the reattachment being predicted too late is that most of the current models and methods predicted turbulent shear stress to be too small in magnitude in the separated region.

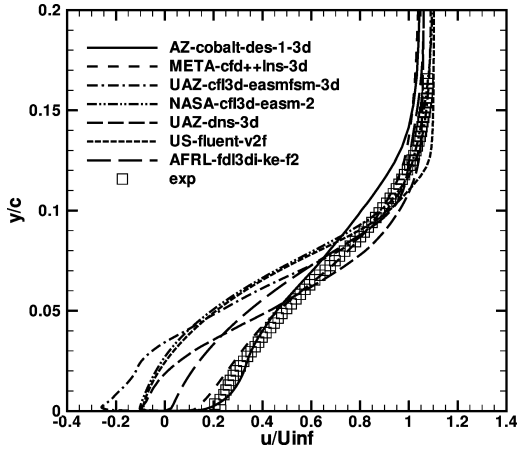

Fig. 25 Sample of case 3 no-flow-control condition u-velocity profiles at $x/c = 1.2$ (downstream of experimental reattachment).

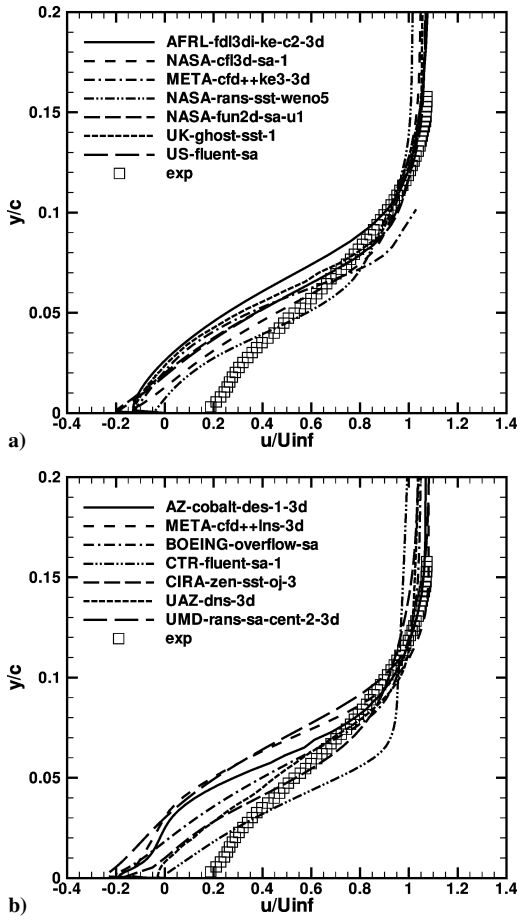

Fig. 26 Sample of case 3 suction condition u-velocity profiles at $x/c = 1.0$ (downstream of experimental reattachment); for ease of readability, results are divided into two figures.

As an illustration of this tendency, Fig. 27 shows both u velocity and turbulent shear stress for the suction condition at the location $x/c = 0.8$, using several representative solutions. The computed velocity profiles exhibited different shapes, especially near the center of the profile, but the overall agreement with experimental results was fairly good for the RANS methods. However, the magnitude of the turbulent shear stress was seriously underpredicted. The turbulent shear-stress data had a maximum uncertainty error of as much as $\pm 10\%$; representative error bars are given in the figure. Even taking into account experimental uncertainty, the results still indicated a large difference between CFD and experiment. One of the anomalies evident in the submissions was that the US-fluent results consistently yielded significantly larger in magnitude turbulent shear-stress levels, in better agreement with experimental data, even though they used many of the same turbulence models as other codes. In any case, the US-fluent solutions still predicted reattachment too far downstream, similar to the other submissions.

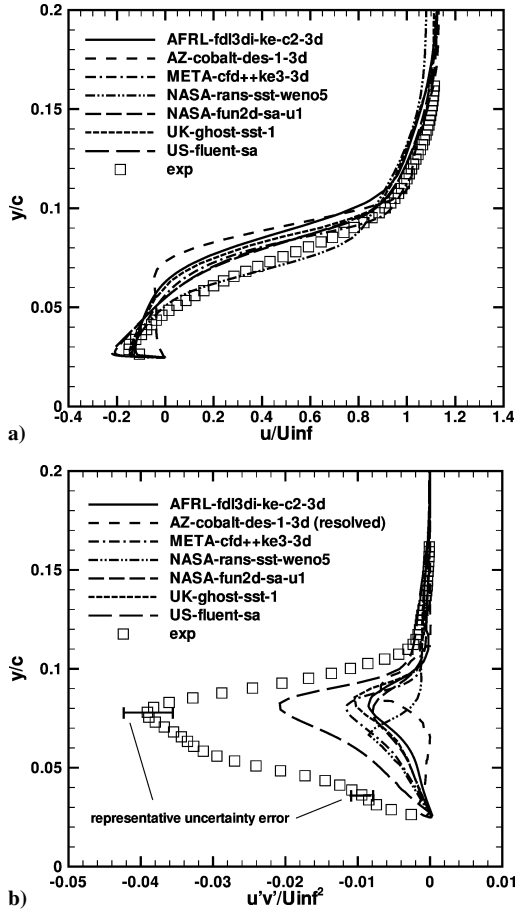

Fig. 27 Sample of case 3 suction condition results at $x/c = 0.8$ (inside separation bubble): a) u velocity and b) turbulent shear stress.

The DNS and blended RANS–LES solutions that reported skin friction were generally on a par with the RANS methods; they, too, predicted reattachment too far downstream. However, DNS- and LES-type models involve typically finer grids than RANS methods and require very lengthy run times. It is possible that future improvements can result from additional efforts in these areas. As shown earlier in Fig. 25, a few of the blended RANS-LES models appeared to do a better job predicting velocity profiles near to and downstream from reattachment than the RANS methods for the no-flow-control condition, but they did not improve results for the suction condition. Also, although not shown, AZ-cobalt-des predicted resolved turbulent shear-stress levels downstream from reattachment (for both no-flow-control and suction conditions) that were much higher in magnitude than most RANS results.

Many of the contributors investigated the effect of grid on the solution, for the no-flow-control and suction conditions. For two dimensions, they noted little influence (all used a minimum of about 50,000 grid points). The influence of turbulence model has been shown earlier in Figs. 22 and 23. Generally, there were some differences between the models as expected, but all performed poorly when it came to predicting reattachment location. No one model stood out as performing consistently better for this case. A few contributors ran without modeling the cavity. In general this did not appear to either help or hurt, even for the suction case. CIRA-zen found that applying oblique suction improved results over applying normal suction.

Figure 28 shows a summary of all of the CFD results for the (optional) oscillatory control case. There was variation among the

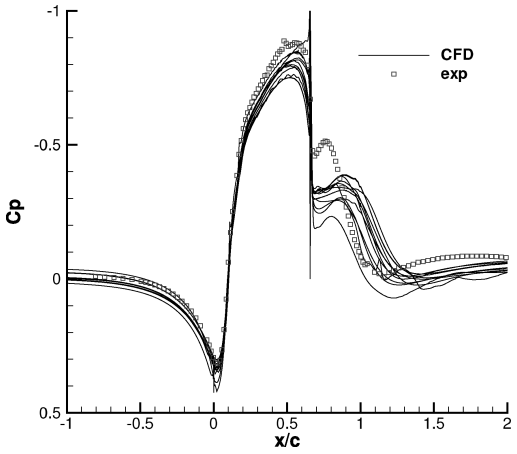

Fig. 28 Summary of case 3 long time-average *Cp* results for oscillatory control condition.

CFD results, but in general they all exhibited similar trends. The results whose separated region pressure recovery occurred farthest upstream (in better agreement with experimental data) were UAZ-cfl3d, BOEING-overflow, and UMD-rans. NASA-fun2d investigated the effect of time step on this solution (between 200 and 400 time steps per cycle) and found very little effect.

VI. Summary

Time-dependent flows involving unsteady flow control are difficult not only to compute with CFD but also to measure experimentally. The CFDVAL2004 workshop in many ways ended up being as much of a workshop on experimental issues as on CFD issues. From the two cases involving synthetic jets (cases 1 and 2), the participants learned that there are still some inconsistencies between different measurement techniques for certain aspects of these types of time-dependent flows. These differences were openly reported at the workshop, to foster honest and open dialog and to help encourage collaborative efforts to work toward improving future results. Most importantly, the workshop proved to be an ideal setting for providing a quality technical interchange between CFD and experimental scientists, where each could learn about the capabilities and limitations inherent in the processes and tools of the other.

This paper focused on providing a summary of the CFD results from the workshop. CFD variation was fairly large. However, trends could still be noted, including overall capabilities and shortcomings. Many of the workshop participants suggested that, now that the workshop has established a baseline for these cases, future CFD efforts should attempt to minimize known sources of CFD variation, especially regarding boundary conditions. It was also suggested that future experiments focus additional effort documenting the time-dependent boundary conditions, especially at and near the exit plane of the jet or suction slot or orifice.

The bottom line from the CFD results can be summed up as follows: no one CFD technique excelled above others, and there was wide variation (especially for time-dependent results) and only qualitative agreement with experimental data. In other words, the "state-of-the-art" CFD methods of today are not fully adequate to consistently and accurately predict these types of flows. What is today's state of the art? Most of the contributors used URANS for the time-dependent cases and RANS to compute the steady cases. A wide variety of turbulence models were employed. Most CFD methods were second order in space and time. Some contributors used higher order, but there did not appear to be any obvious benefits from doing so for these cases. Most contributors utilized transpiration boundary conditions on a fixed grid to simulate moving walls. The few blended RANS–LES, LES, and DNS solutions showed merit and were of similar quality to the RANS and URANS solutions. With today's increased computer power and improved algorithms, these advanced methods are currently coming of age and represent the way much of CFD will be performed in the future. However, as yet they show no clear benefits over RANS/URANS in the sense of providing consistently better results for the workshop cases.

Case 1 (synthetic jet into quiescent air) was a difficult experiment to simulate. The flowfield was probably mostly laminar or transitional, and so it was unclear how best to simulate it. Also, although the case was nominally two-dimensional at the slot center near the wall, it is likely that three-dimensional effects from the slot ends had an influence higher in the flowfield. The piezoelectric driver used in the experiment was difficult to model using CFD because it moved like a drum (and possibly with multiple shape modes) and not like a rigid piston. The experiment indicated a deviation from periodicity in the velocity near the jet exit that was not completely simulated or captured by the CFD results and caused specific phase results to be misaligned. Except for a few cases, CFD usually somewhat overpredicted average jet width in the near field. In the URANS simulations, turbulence models were found to have a significant effect for this case. In general, the $k-\varepsilon$, SA, and SST models performed better compared to experimental data than other models tested.

Case 2 (synthetic jet in a crossflow) was the least computed of the three cases, probably owing to its being both time-dependent and (necessarily) three-dimensional. Similarly to case 1, the time-dependent experimental velocities measured near the orifice exit exhibited anomalies not captured or modeled by CFD. In particular, the experiment exhibited a dip in vertical velocity on the downstroke and a very large spanwise velocity component during the expulsion part of the cycle that none of the CFD methods accounted for. In spite of this, the participants obtained reasonably good qualitative results compared to experimental results, but there were significant CFD variations in both the long-time-average and the phase-averaged results. No one method, algorithm, or turbulence model stood out as being the best methodology. Generally, different turbulence models for URANS did not have as much of an impact on this case as different grids, codes, and other solution variations.

Case 3 (flow over a hump model) had the greatest number of workshop participants because the required cases were nominally steady and two-dimensional. However, it was discovered after the workshop that the side plates used in the tunnel caused blockage that, if not modeled or accounted for, resulted in relatively minor (but noticeable) overprediction of the pressures over most of the hump. Overall, case 3 was not a severe test from the point of view of predicting separation, but CFD results were deficient in another important regard: they consistently predicted the reattachment location to be significantly farther downstream than the location documented in the experiment. This same behavior occurred regardless of turbulence model or method; even a DNS computation (underresolved very near the wall) predicted too long of a separation bubble. Inside the bubble itself, most computations predicted velocity profiles in reasonably good agreement with experimental data but underpredicted turbulent shear stresses in magnitude. This underprediction is consistent with delayed reattachment because it indicates reduced turbulent mixing inside the separated region compared with experimental data.

In conclusion, the CFDVAL2004 workshop has established a benchmark for three different flows involving synthetic jets and turbulent separation control. Although the current state-of-the-art CFD methods are deficient in being able to consistently and accurately predict these flows, two areas have been identified as key to improvement:

1) First, for synthetic jets it is important to employ consistent boundary conditions when comparing multiple CFD methods, and grid-resolution studies should always be conducted. Only then will one be able to isolate and work to correct deficiencies in the CFD models and methods. Implicit in this need is the requirement that experiments be used to document extremely detailed and accurate time-dependent flowfield variables at and near the slot or orifice exits.

2) Second, for the hump model case turbulence models (for RANS) or other methods, such as blended RANS–LES, need to be improved, developed, or calibrated to increase the mixing in the separated region and bring about earlier reattachment and flow recovery.

Acknowledgments

The authors thank H. Atkins, P. Balakumar, and M. Carpenter of NASA Langley Research Center for their valuable contributions and useful discussions during the planning and execution of the CFDVAL2004 workshop. Also, the authors acknowledge J. Sawyer and P. Greene of NASA Langley Research Center for their help and expertise in arranging and carrying out many particulars involved in the organization of the workshop.

References

[1]Lachmann, G. V., *Boundary Layer and Flow Control. Its Principles and Application*, Vol. 1, Pergamon, New York, 1961.

[2]Seifert, A., Darabi, A., and Wygnanski, I., "Delay of Airfoil Stall by Periodic Excitation," *Journal of Aircraft*, Vol. 33, No. 4, 1996, pp. 691–698.

[3]Smith, B. L., and Glezer, A., "The Formation and Evolution of Synthetic Jets," *Physics of Fluids*, Vol. 10, No. 9, 1998, pp. 2281–2297.

[4]Amitay, M., Smith, D. R., Kibens, V., Parekh, D. E., and Glezer, A., "Aerodynamic Flow Control over an Unconventional Airfoil Using Synthetic Jet Actuators," *AIAA Journal*, Vol. 39, No. 3, 2001, pp. 361–370.

[5]Gordon, M., and Soria, J., "PIV Measurements of a Zero-Net-Mass-Flux Jet in Cross Flow," *Experiments in Fluids*, Vol. 33, No. 6, 2002, pp. 863–872.

[6]Smith, D. R., "Interaction of a Synthetic Jet with a Crossflow Boundary Layer," *AIAA Journal*, Vol. 40, No. 11, 2002, pp. 2277–2288.

[7]Greenblatt, D., and Wygnanski, I. J., "The Control of Flow Separation by Periodic Excitation," *Progress in Aerospace Sciences*, Vol. 36, No. 7, 2000, pp. 487–545.

[8]Mittal, R., Rampunggoon, P., and Udaykumar, H. S., "Interaction of a Synthetic Jet with a Flat Plate Boundary Layer," AIAA Paper 2001-2773, June 2001.

[9]Huang, L., Huang, G., LeBeau, R., and Hauser, T., "Optimization of Blowing and Suction on NACA 0012 Airfoil Using Genetic Algorithm," AIAA Paper 2004-0225, Jan. 2004.

[10]Ravi, B. R., Mittal, R., and Najjar, F. M., "Study of Three-Dimensional Synthetic Jet Flowfields Using Direct Numerical Simulation," AIAA Paper 2004-0091, Jan. 2004.

[11]Yamaleev, N. K., and Carpenter, M. H., "A Reduced-Order Model for Efficient Simulation of Synthetic Jet Actuators," NASA TM-2003-212664, Dec. 2003.

[12]Viken, S. A., Vatsa, V. N., and Rumsey, C. L., "Flow Control Analysis of the Hump Model with RANS Tools," AIAA Paper 2003-0218, Jan. 2003.

[13]Agarwal, R., Vadillo, J., Tan, Y., Cui, J., Guo, D., Jain, H., Cary, A., and Bower, W., "Flow Control with Synthetic and Pulsed Jets: Applications to Virtual Aeroshaping, Thrust-Vectoring, and Control of Separation and Cavity Oscillations," AIAA Paper 2004-0746, Jan. 2004.

[14]Yao, C. S., Chen, F. J., Neuhart, D., and Harris, J., "Synthetic Jet Flow Field Database for CFD Validation," AIAA Paper 2004-2218, June–July 2004.

[15]Schaeffler, N. W., and Jenkins, L. N., "The Isolated Synthetic Jet in Crossflow: A Benchmark for Flow Control Simulation," AIAA Paper 2004-2219, June–July 2004.

[16]Greenblatt, D., Paschal, K. B., Schaeffler, N. W., Washburn, A. E., Harris, J., and Yao, C. S., "A Separation Control CFD Validation Test Case. Part 1: Baseline and Steady Suction," AIAA Paper 2004-2220, June–July 2004.

[17]Greenblatt, D., Paschal, K. B., Yao, C. S., and Harris, J., "A Separation Control CFD Validation Test Case. Part 2: Zero Efflux Oscillatory Blowing," AIAA Paper 2005-0485, Jan. 2005.

[18]Rumsey, C. L., Gatski, T. B., Sellers, W. L., III, Vatsa, V. N., and Viken, S. A., "Summary of the 2004 CFD Validation Workshop on Synthetic Jets and Turbulent Separation Control," AIAA Paper 2004-2217, June–July 2004.

T. Beutner
Guest Editor